(2)

Report N00014-88-C-0403F

DEVELOPMENT OF N_2 SENSOR FOR *IN VIVO* MEASUREMENT OF PN_2 IN BIOLOGICAL TISSUES

CONTRACT N00014-88-C-0403

Principal Investigator: L. S. Robblee
Staff Scientists: M. M. Brunelle
R. B. Jones

Performance Site: EIC Laboratories, Inc.
111 Downey Street
Norwood, Massachusetts 092062

March, 1992

Final Report for Period 1 August 1988 - 31 October 1991
Approved for Public Release - Distribution Unlimited

Prepared for:

Naval Medical Research and Development
Command, NMC, NCR
Bethesda, Maryland 20889-5044

UNCLASSIFIED
SECURITY CLASSIFICATION OF THIS PAGE

REPORT DOCUMENTATION PAGE

1a. REPORT SECURITY CLASSIFICATION UNCLASSIFIED	1b RESTRICTIVE MARKINGS N/A
2a. SECURITY CLASSIFICATION AUTHORITY N/A 2b. DECLASSIFICATION/DOWNGRADING SCHEDULE N/A	3 DISTRIBUTION/AVAILABILITY OF REPORT Approved for Public Release; Distribution Unlimited
4. PERFORMING ORGANIZATION REPORT NUMBER(S) C897F	5. MONITORING ORGANIZATION REPORT NUMBER(S)
6a NAME OF PERFORMING ORGANIZATION EIC Laboratories, Inc. 6b. OFFICE SYMBOL (If applicable) 1L930	7a NAME OF MONITORING ORGANIZATION Naval Medical Research and Development Command, NMC, NCR
6c. ADDRESS (City, State, and ZIP Code) 111 Downey Street Norwood, MA 02062	7b. ADDRESS (City, State, and ZIP Code) Bethesda, MD 20889-5044
8a. NAME OF FUNDING/SPONSORING ORGANIZATION NMRDC 8b. OFFICE SYMBOL (If applicable) N00075	9. PROCUREMENT INSTRUMENT IDENTIFICATION NUMBER Contract No. N00014-88-C-0403
8c. ADDRESS (City, State, and ZIP Code) Bethesda, MD 20889-5044	10. SOURCE OF FUNDING NUMBERS PROGRAM ELEMENT NO. PROJECT NO. TASK NO. WORK UNIT ACCESSION NO.

11. TITLE (Include Security Classification) Development of N_2 Sensor for In Vivo Measurement of PN_2 in Biological Tissues

12. PERSONAL AUTHOR(S) Lois S. Robblee, Michele M. Brunelle, Rochelle B. Jones

13a. TYPE OF REPORT Final Report	13b. TIME COVERED FROM Aug 88 TO Oct 91	14. DATE OF REPORT (Year, Month, Day) 1992 March 18	15 PAGE COUNT

16. SUPPLEMENTARY NOTATION

17. COSATI CODES

FIELD	GROUP	SUB-GROUP

18. SUBJECT TERMS (Continue on reverse if necessary and identify by block number) Nitrogen sensor, nitrogen electrode, PN_2 measurement, nitrogen tension, microelectrodes, electrode array, electrochemical sensor, Nafion, dinitrogen complex, ruthenium-dinitrogen complex.

19. ABSTRACT (Continue on reverse if necessary and identify by block number)

An electrochemical sensor for nitrogen was developed based on the kinetics of the reaction of a transition metal cation, ruthenium (II) aquopentaammine, with molecular dinitrogen. Prototype PN_2 sensors were fabricated which incorporate an array of carbon microdisks as the active electrode surface with the smallest probe diameter equivalent to a 23 gauge hypodermic needle. Sensors were characterized on the basis of their electrochemical responses for a diffusion controlled process, the kinetics of the Ru^{II}-N_2 complexation reaction, and their operating performance in measuring PN_2. *In vitro* performance tests under equilibrium conditions demonstrated a linear response over a PN_2 range of 1 to 10 atm. Iterative PN_2 measurements had a ± 5% reproducibility with equilibrium PN_2 of 0.77 or 1 atm. Under dynamic conditions of changing PN_2, the sensor response indicated that the actual concentration of dissolved N_2 equilibrates slowly with changes in N_2 pressure in the gas phase above the solution, with washout occurring more slowly than washin. Electroanalytical protocols which were satisfactory for early prototypes based on large glassy carbon electrodes must be modified for use with the microdisk array sensors due to the different mass transport properties of microelectrode arrays. Development of standard protocols and a user interface would enhance the utility of the sensor technology to the hyperbaric medical research community.

20. DISTRIBUTION/AVAILABILITY OF ABSTRACT ☒ UNCLASSIFIED/UNLIMITED ☐ SAME AS RPT. ☐ DTIC USERS	21. ABSTRACT SECURITY CLASSIFICATION UNCLASSIFIED	
22a. NAME OF RESPONSIBLE INDIVIDUAL Peter D. Kent, CDR, MC, USN	22b. TELEPHONE (Include Area Code) (301) 295-1468	22c. OFFICE SYMBOL N00075

DD FORM 1473, 84 MAR
83 APR edition may be used until exhausted.
All other editions are obsolete
SECURITY CLASSIFICATION OF THIS PAGE
☆ U.S. Government Printing Office: 1986-607-044
UNCLASSIFIED

TABLE OF CONTENTS

LIST OF ILLUSTRATIONS

LIST OF TABLES

1.0 INTRODUCTION

This report describes work carried out under Office of Naval Research Contract N00014-88-C-0403 during the period August 1, 1988 to October 31, 1991. The three year program of research was undertaken to develop and test an electroanalytical system for *in vivo* quantitation of tissue PN_2. Because molecular dinitrogen is not readily oxidized or reduced in an aqueous solvent, the key to developing an electrochemical sensor for N_2 was to identify a reaction involving dinitrogen, the progress of which could be followed with electrochemical methods. The electrochemical sensor developed at EIC Laboratories is based on the kinetics of the reaction of molecular dinitrogen with a transition metal cation, ruthenium (II) aquopentaammine, $[Ru(NH_3)_5H_2O]^{+2}$ [1,2]. Work carried out under previous programs demonstrated that PN_2 could be quantified by measuring the rate of Ru pentaammine dinitrogen complex formation [3,4,5,6].

The finalized electroanalytical system will include the following elements: a) the PN_2 sensor consisting of a N_2-sensing, an auxiliary current carrying electrode, and a reference electrode; b) an external electronic unit for automated electrochemical control and data acquisition; and c) an interface between the control unit and the PN_2 sensor. The key component of this system, to be developed under this contract, is the N_2 sensing electrode. It must be capable of measuring accurately and reliably changes in PN_2 in a system undergoing atmospheric compression and decompression. In order to accomplish this goal, the program was organized into five specific tasks:

1. Select an electrode material and Ru cation/polymer combination which demonstrates durability of the Ru cation/polymer system and optimum electron transfer kinetics, gas diffusion properties, and kinetics of Ru-N_2 complex formation. Additionally, the materials must possess the physical and mechanical properties suitable for fabrication into an implantable sensor.

2. Design and fabricate prototype PN_2 sensor assemblies consisting of a N_2 sensing electrode, auxiliary electrode and reference electrode.

3. Test prototype N_2-sensing electrodes and PN_2 sensor assemblies in a simulated *in vivo* test medium at pressures up to 10 atm. Develop performance specifications for *in vivo* testing.

4. Optimize the electroanalytical waveform to enable fast, iterative measurements of PN_2 with computer control of signal generation, data acquisition and data analysis.

5. Collaborate with the Hyperbaric Medicine Program Center, NMRI, Bethesda, MD for evaluation of N_2 sensing ability in their experimental protocol.

The three year program accomplished all of the proposed tasks with the exception of Task 4 and the *in vivo* aspects of Task 5. The program concluded with the availability of a prototype nitrogen sensor which can be fabricated to the size of a 16, 23, or 20 gauge hypodermic needle (o.d. = 1.6 mm, 0.9 mm and 0.6 mm, respectively). Iterative PN_2 measurements obtained with a sensor in the 16 gauge size have a reproducibility of ± 5% with equilibrium PN_2 of 0.77 or 1 atm. Under dynamic conditions of changing PN_2, the sensor response indicates that the actual concentration of dissolved N_2 equilibrates slowly with changes in N_2 pressure in the gas phase above the solution, with N_2 washout occurring more slowly than washin. In the report that follows, the theory and general procedures of nitrogen sensor operation are reviewed in Section 2.0. Section 3.0 summarizes the development of the PN_2 sensor. Section 4.0 describes the performance of prototype PN_2 sensors.

2.0 THEORY OF NITROGEN SENSOR OPERATION

2.1 Mechanism

The EIC nitrogen sensor is based on the following series of reactions which are carried out within a Nafion film on the surface of the sensor:

1) Formation of the N_2-complexing cation $[Ru(NH_3)_5H_2O]^{+2}$.

a. $[Ru(NH_3)_5Cl]^{+2} + e^- \rightarrow [Ru(NH_3)_5Cl]^{+1}$ (reduction at E_{red})

b. $[Ru(NH_3)_5Cl]^{+1} + H_2O \rightarrow [Ru(NH_3)_5H_2O]^{+2} + Cl^-$ (aquation)

2) Formation of the ruthenium dinitrogen complex.

$[Ru(NH_3)_5H_2O]^{+2} + N_2 \rightarrow [Ru(NH_3)_5N_2]^{+2}$ (chemical reaction)

3) Oxidization of uncomplexed Ru (II) cation.

$[Ru(NH_3)_5H_2O]^{+2} \rightarrow [Ru(NH_3)_5H_2O]^{+3} + e^-$ (oxidation at $E_{ox(RuII)}$)

4) Oxidation of ruthenium dinitrogen complex.

a. $[Ru(NH_3)_5N_2]^{+2} \rightarrow [Ru(NH_3)_5N_2]^{+3}$ (oxidation at $E_{ox(RuII\text{-}N2)}$)

b. $[Ru(NH_3)_5N_2]^{+3} \rightarrow [Ru(NH_3)_5H_2O]^{+3} + N_2$ (decomposition)

In addition to the above reactions, ruthenium dinitrogen complex can react with $[Ru(NH_3)_5H_2O]^{+2}$ to form a binuclear complex, bis-ruthenium dinitrogen dimer according to:

5) $[Ru(NH_3)_5H_2O]^{+2} + [Ru(NH_3)_5N_2]^{+2} \rightarrow [(Ru(NH_3)_5)_2N_2]^{+4}$ (dimerization)

2.2 Kinetics

From reaction (2):[1]

$$\frac{d[Ru^{II}-N_2]}{dt} = k[Ru^{II}][N_2]. \qquad [1]$$

---

[1] To enhance readability, the following abbreviations will be used henceforth:

Ru^{III}:	$[Ru(NH_3)_5Cl]^{+2}$.
Ru^{II}:	$[Ru(NH_3)_5H_2O]^{+2}$.
Ru^{II}-N_2:	$[Ru(NH_3)_5N_2]^{+2}$.
Ru^{II}-N_2-Ru^{II}:	$[Ru(NH_3)_5N_2Ru(NH_3)_5]^{+4}$

Since $[N_2]$ is essentially constant compared to $[Ru^{II}]$, the reaction follows pseudo-first order kinetics, and the rate expression can be written as:

$$\frac{d[Ru^{II}-N_2]}{dt} = k'[Ru^{II}], \quad \text{where} \tag{2}$$

$$k = k'/[N_2] \quad (M^{-1}sec^{-1}). \tag{3}$$

Pseudo-first order kinetics of reaction (2) permit the experimental determination of k′ from the ratio of initial $[Ru^{II}]$ to $[Ru^{II}]$ at *t* seconds according to the relationship:

$$k't = \ln\frac{[Ru^{II}]_0}{[Ru^{II}]_t} \tag{4}$$

or

$$\ln[Ru^{II}]_t = -k't + \ln[Ru^{II}]_0 \tag{5}$$

In prior studies of reaction (2) in homogeneous solutions, k′ was determined from linear plots of ln $[Ru^{II}\text{-}N_2]$ *vs* time [7] or ln $[Ru^{II}]$ *vs* time [5] according to the relationship in equation [5]. The reaction was demonstrated to be first order with respect to $[N_2]$ by determining k′ at various concentrations of dissolved $[N_2]$. The second order rate constants, measured in these studies from the slopes of ln k′ *vs* ln PN_2 plots, were 0.079 M^{-1} sec^{-1} [7] and 0.056 M^{-1} sec^{-1} [5].

The previous solution studies of $Ru^{II}\text{-}N_2$ complex formation [5,7] also demonstrated that the formation of the dimer according to reaction (5) was first order with respect to $[Ru^{II}]$ and $[Ru^{II}\text{-}N_2]$, and was detected in ln $[Ru^{II}]$ *vs* time plots by an increase in slope due to participation of Ru^{II} in both reactions (2) and (5). In the operation of the EIC nitrogen sensor, it is important that reaction (5) not occur during the time of measurement because it will result in artifactually high values for k′.

2.3 Generalized Protocol for Measuring k′ and PN_2.

The general protocol for carrying out PN_2 measurements with the EIC nitrogen sensors is summarized in Table 1. The potential waveform and the corresponding current response of the sensor during each phase of the measurement protocol are shown in Figure 1. All of the performance tests of EIC nitrogen sensors were carried out using this protocol, with the reaction times and the number of reactions varied as part of the effort to establish the optimum conditions for PN_2 analysis.

Table 1. Procedure for Determining PN_2 with EIC Nitrogen Sensor

1. Reaction Step	Hold the electrode potential at E_{red} for some time, $t_{reaction}$. During this time, Ru^{II} produced by the electroreduction of Ru^{III} will react (chemically) with N_2 to form a Ru^{II}-N_2 complex.
2. Measurement Step	Scan the electrode potential to $E_{ox(RuII)}$. Only uncomplexed Ru^{II} will be oxidized at this potential. The magnitude of the current response is proportional to the quantity of <u>uncomplexed</u> Ru^{II}.
3. Repeat Sequence	Repeat steps 1 and 2, *N* times, to allow a total reaction time of $Nt_{reaction}$ seconds and obtain incremental measurements of uncomplexed Ru^{II}.
4. Regeneration Step	Scan the electrode potential to $E_{ox(RuII\text{-}N2)}$ to oxidize all the Ru^{II}-N_2 that formed during *N* reaction sequences, and regenerate Ru^{III}, in preparation for another sequence of measurements.
5. Data Analysis	The pseudo-first order rate constant, k', is determined from the linear plot of $\ln[Ru^{II}]$, as measured in Steps 1-3, *vs* the aggregate reaction time. With a known $[N_2]$, calculate the second order rate constant, k ($[N_2]^{-1}$ sec^{-1}) from $k = k'/[N_2]$
6. For unknown $[N_2]$.	Repeat steps 1-5 to find k'_{new}. Using k determined with a known $[N_2]$, calculate $[N_2]_{new}$ from $[N_2]_{new} = k'_{new}/k$.

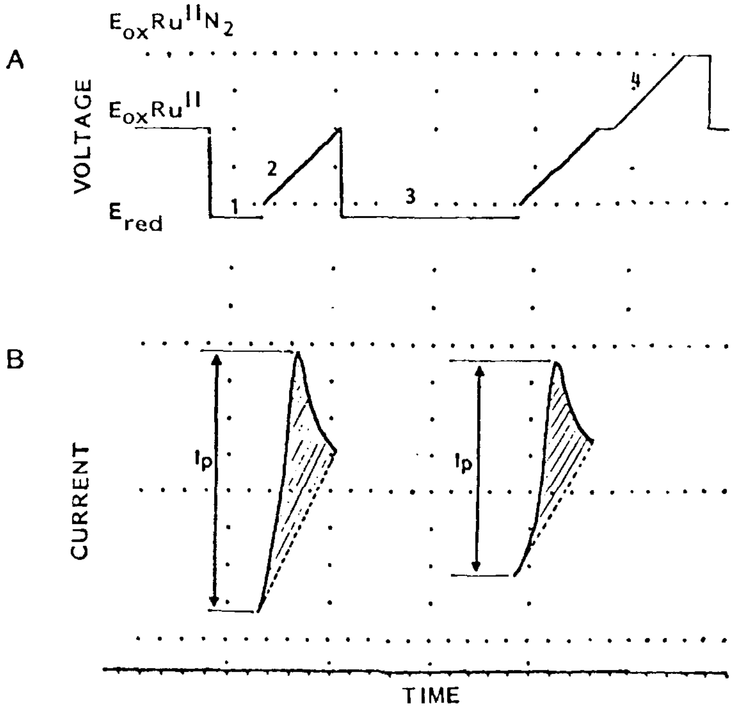

Figure 1. Potential waveform (A) and corresponding current response (B) of an EIC nitrogen sensor during measurements of PN_2. [Ru^{II}] is quantitated by measuring the magnitude of the current peak, i_p, or by integrating the area under the curve (shaded). Numerals in the potential waveform correspond to the steps in the protocol listed in Table 1.

3.0 FABRICATION OF NITROGEN SENSORS

3.1 First Nitrogen Sensor Prototype.

The first prototype of the nitrogen sensor consisted of a 3 mm diam. glassy carbon (GC) rod mounted in a Kel-F holder. The surface of the GC electrode was polished prior to use to give a smooth, mirror-like finish. To prepare the GC electrode for nitrogen measurements, it was coated with a thin film of the perfluorosulfonate polymer, Nafion (NAF) (DuPont). The polymer was applied to the GC surface from an ethanol/water solution by micropipette, and allowed to dry thoroughly. The GC/NAF electrode was then soaked in a dilute solution of Ru^{III} cation to incorporate the Ru^{III} cation into the Nafion polymer by ion exchange.

Testing of this prototype electrode was performed in a Parr pressure reactor fitted with electrical feed-throughs for electrode connections. The test electrode, a reference electrode and auxiliary electrode were immersed in ~100 mls of electrolyte solution. A magnetic stirrer was used in the bulk electrolyte to promote rapid equilibration between gas and aqueous phase. Before studying reaction kinetics at various PN_2, gas at elevated pressure was allowed to equilibrate for at least 20 minutes before acquiring data. The electrochemical instrumentation consisted of a potentiostat, function generator to generate the required potential steps and ramps, and a recorder to record the current response of the electrode. Figure 2 illustrates the three-electrodes as they were mounted in the pressure chamber.

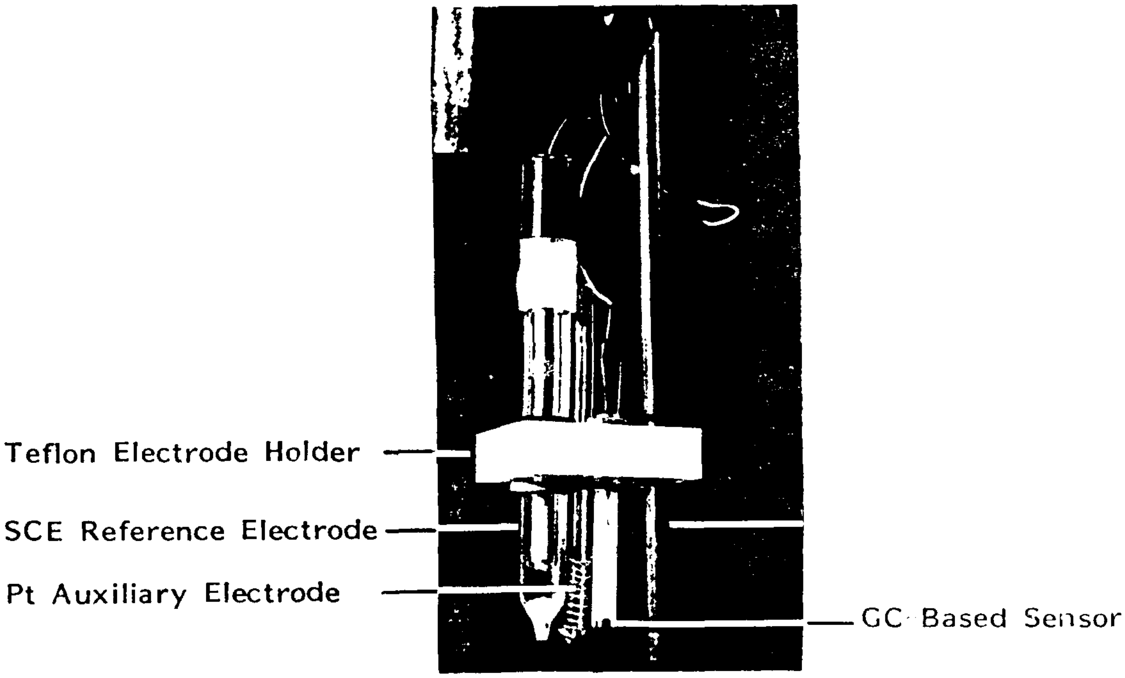

Figure 2. Three electrode arrangement for PN_2 measurements with first prototype nitrogen electrode.

The stability of Ru cation binding in Nafion was evaluated under different conditions of electrode potential, gas composition and electrolyte composition. Ru efflux from Nafion-coated glassy carbon electrodes followed first order kinetics with plots of ln [Ru] vs time being linear over the total time of an experiment (up to 5 hrs in a single day). Rate constants for Ru efflux from several Nafion-coated electrodes are given in Table 2. Pure efflux was unaffected by gas composition, e.g., Ar or N_2 saturation. Electrolyte pH or Cl^- presence also had little effect. In contrast, electrode potential had a significant effect on the efflux rate, which was likely related to the oxidation state of the metal center and the charge on the cation. The efflux rate was slowest when the Ru cation was in its highest oxidation state, as when the electrode was held at 0.0 V *vs* SCE or at open circuit. Intermediate efflux rates were observed when the electrode potential was alternated between -0.5 V and 0.0 V *vs* SCE.

Table 2. Efflux Rates of Ru from Nafion-Coated Electrodes

Electrolyte	Efflux Rate (min^{-1})		
	0.0 V *vs* SCE	-0.5 V *vs* SCE	
		Intermittent	Constant
0.1 M H_2SO_4	1.4×10^{-3}	7.7×10^{-3}	3.9×10^{-2}
"	2.5×10^{-3}	7.8×10^{-3}	not measured
"	3.8×10^{-3}	1.6×10^{-2}	not measured
0.13 M NaCl	1.4×10^{-3}	not measured	not measured

The lowest efflux rate corresponded to about 8 hr half-life for the Ru-Nafion binding which might be adequate for short term PN_2 measurements. Multiple layers of Nafion provided some improvement in retarding the efflux rate, however it was still not possible to obtain a reliable estimate of k′ for Ru^{II}-N_2 complex formation by measuring the decrease in $[Ru^{II}]$. Consequently, a major change in the configuration of the nitrogen sensor was undertaken.

3.2 Improved Glassy Carbon-Based Nitrogen Sensor Designs.

Improved durability of the Nafion binding of Ru cations was achieved by combining the three electrodes, GC, reference and auxiliary electrodes, into a single unit, coating the electrodes with Nafion to provide ionic continuity for current flow, and encapsulating the entire assembly within a hydrophobic membrane permeable to gas but not to water and ions, e.g., Teflon. This strategy prevented the efflux of Ru from the Nafion and increased the useful lifetime of the sensor to more than 4 days. An additional benefit of isolating the sensing elements within the Teflon membrane is that Teflon provides an excellent biocompatible barrier between tissue components and sensor elements.

Two designs of GC-based sensor were fabricated, differing only in the diameter of the GC working electrode. In one design, the 3 mm diam. GC rod was insulated with multiple coats of an epoxy varnish (Epoxylite). In the second design, the 3 mm GC rod was first ground to a conical tip. The tip was embedded in epoxy, baked at 80°C to cure the epoxy, and polished to expose a small diameter (~0.6 mm) GC surface. The remainder of the construction of the two sensors is nearly the same. Two pieces of Pt foil with Pt lead wires fused to them were attached to each side of the GC rod and held in place with shrink tubing. These pieces of foil were not allowed to contact each other or the bare GC surface. Windows were cut in the shrink tubing to expose some of the underlying Pt so that these could serve as auxiliary and quasi-reference electrodes. The windows were sized so that the area of the auxiliary electrode would be ~3 times larger than the GC cross-sectional surface area. Electrical connection was made to the GC via a socket connector. To prepare this sensor for use, the GC surface was polished to a mirror finish using graded sizes of diamond polishing compounds and sonicating in several changes of 2X distilled water between each polishing step. A Nafion coating was applied by dipping a sensor into a solution of Nafion in ethanol to obtain a continuous film covering the surfaces of the GC and the two Pt electrodes. Nafion concentrations of 2-5% seemed optimum. After drying in air for 30-60 min, a Nafion-coated sensor was placed in a 0.25 mM solution of $[Ru(NH_3)_5Cl]^{+2}$ in 1 M H_2SO_4 to load the Nafion film with $[Ru(NH_3)_5Cl]^{+2}$ by ion exchange. The uptake of $[Ru(NH_3)_5Cl]^{+2}$ into the Nafion film was followed by cyclic voltammetry [6]. When $[Ru(NH_3)_5Cl]^{+2}$ uptake was complete, the sensor was capped with a Goretex membrane which was held in place with a band of plastic tubing.

3.3 Carbon Fiber Nitrogen Sensors.

In order to decrease the overall size of the sensors, a 10 μm diameter carbon fiber electrode was used as the voltammetry electrode in place of the GC electrode used previously. The carbon fiber electrode and two Pt wires serving as auxiliary and quasi-reference electrodes were encapsulated with a quick-setting epoxy. When the tip of the assembly was coated with Nafion and covered with a hydrophobic cap, the overall diameter was ~1.2 mm., small enough for some *in vivo* applications. However, this design was ultimately rejected because of the very low current signal of the 10 μm diameter carbon fiber, the fragility of the assembly, and the instability of the quick-setting epoxy over a prolonged period of testing.

The most promising sensor configuration encompasses the use of stainless steel tubing, filled with a slow curing epoxy, as the holder for the voltammetry electrode and the Pt quasi-reference electrode. The use of stainless steel tubing provides physical robustness and the additional benefit that the tubing itself serves as the auxiliary electrode. A bundle of 10-30 carbon fibers, threaded through the bore of the tubing, function together as the voltammetry electrode with a significant improvement in signal-to-noise level. The smallest sized sensor to date was fabricated within a 23 gauge hypodermic needle (0.6 mm. diam). When the hydrophobic membrane cap is added, the sensor has an overall diameter of ~0.8 mm. Further decrease in size may be possible by modification of the fabrication method. The configuration and the performance of the PN_2 microsensors are detailed in the following section.

3.4 PN_2 Microsensor.

3.4.1 Microdisk Array Design.

The PN_2 microsensor is depicted in Figures 3 and 4. A block diagram of the computer-based electrochemical control and data acquisition system is shown in Figure 5. The essential elements of the microsensor are the following:

A. An array of inlaid microfiber carbon electrodes as the working (voltammetry) electrode.

B. An inlaid Pt microdisk electrode as a pseudoreference electrode.

C. A stainless steel cannula containing elements A and B embedded in an epoxy matrix. The cross-sectional surface of the tip of the cannula serves as an auxiliary electrode to complete the electrochemical cell.

D. A membrane of Nafion ion exchange polymer covering the three electrodes and containing the Ru pentaammine reactant and supporting electrolyte.

E. A gas-permeable, hydrophobic membrane cap (Goretex) covering the electrode assembly. The hydrophobic membrane permits exchange of gases but not liquid between the internal sensor compartment and the external environment.

F. Electrical leads from the reference and working electrodes extending from the epoxy are soldered to the pins in one side of a three-circuit connector (not shown in the drawing of Figure 3). A mating connector with lead wires connects the three electrodes of the sensor to the electrochemical control instrumentation.

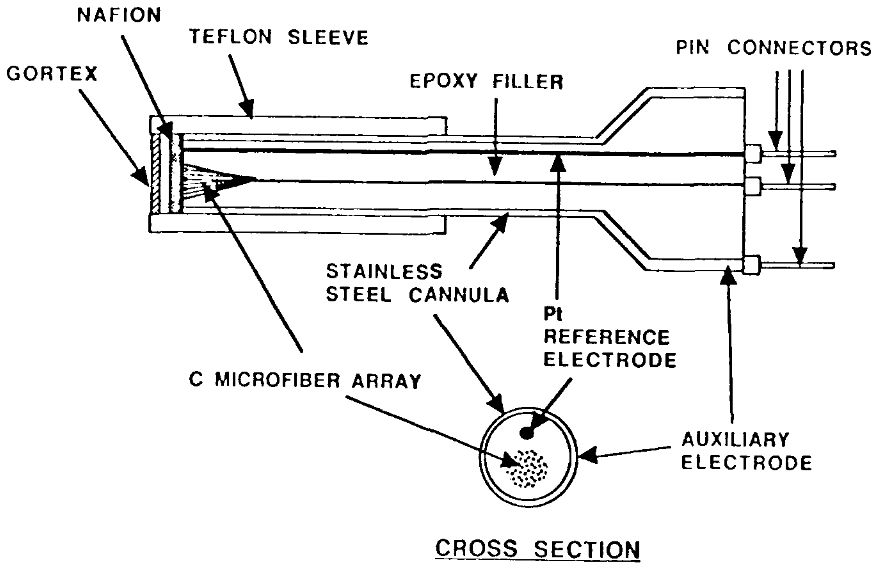

Figure 3. Diagrammatic representation of PN_2 microsensor (not to scale).

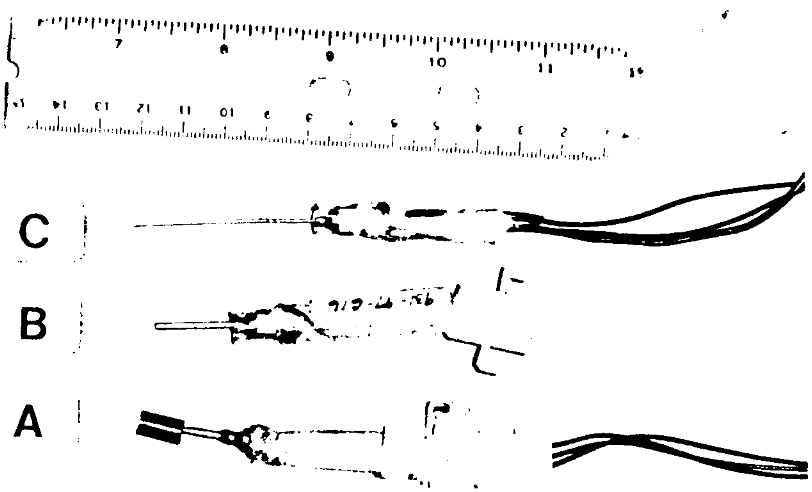

Figure 4. Prototype PN_2 microsensors. *Sensors* A *and* B have probe size of 16 gauge hypodermic needle. Sensor A is shown with attached microcell for *in vitro* testing. Sensor C has probe size of 23 gauge hypodermic needle.

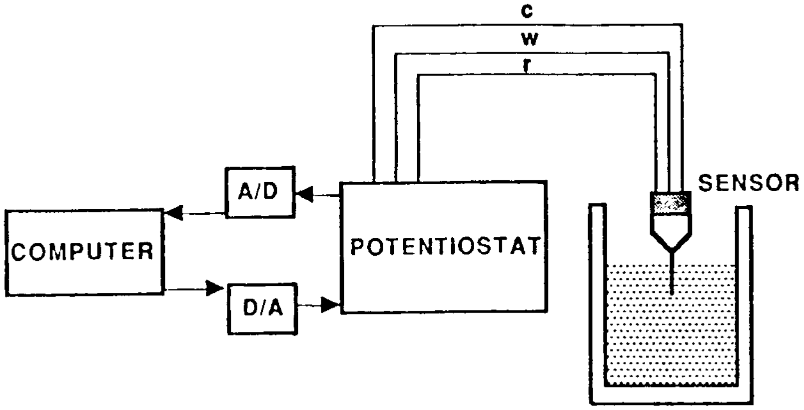

Figure 5. Block diagram of instrumentation for measuring PN_2. A voltage waveform, V-t, is generated by the computer and transmitted to the potentiostat via the D/A converter. The voltage waveform, referenced to some reference electrode (r), is applied to the working electrode (w) via the potentiostat. The current, I, between the counter electrode (c) and (w) is transmitted from the potentiostat to the computer via the A/D converter. Collected data are stored and processed by computer software.

3.4.2 Electrochemical Characterization of Microdisk Array Sensors.

Because of the way in which the microdisk array is assembled, it is difficult to verify optically the total number of fiber cross sections that are exposed at the surface, or the dimensions of the exposed cross sections. Thus, we have used cyclic voltammetric and chronoamperometric measurements based on electrochemical processes controlled by mass transport to obtain estimates of the radius and electrochemical surface area of the microdisk array electrode. Some theoretical background information is presented to provide greater understanding of the methodology employed. This is followed by a brief description of the experimental protocols and the results obtained.

a. Electrochemical Background.

The concept of electrode dimensionality introduced by Oldham provides a convenient way to express the interrelationships between the physical dimensions of an electrode and diffusive transport to the electrode [8]. All electrodes may be characterized by two linear dimensions, x and y, and an area, A, equal to xy times a numerical constant which depends on the shape of the electrode ($A \propto xy$). For an electrochemical process involving diffusion to an electrode the diffusion length, d, must also be considered. This non-geometric dimension equals $(Dt)^{1/2}$, where D is the diffusion coefficient in $cm^2\ sec^{-1}$ of the electroactive solute and t is the time interval for the experiment in sec. The electrode dimensionality depends on the relative magnitude of the geometric dimensions compared to the diffusion length. These relationships can be summarized as follows:

Electrode Dimensionality	Mode of Diffusion	Relationship between Dimensions
{2}	linear	$x \gg d \ll y$
{1}	cylindrical	$x \gg d \gg y$
{0}	spherical	$x \ll d \gg y$

The above relationships demonstrate that the electrode dimensionality depends upon the observation time of the experiment. At relatively short observation times, the dimensionality of all electrodes is {2}. As the time increases, the dimensionality of the electrode may decrease. This concept of electrode dimensionality allows, to a good approximation, electrodes of different shapes to be characterized on the basis of their electrochemical responses to a diffusion-controlled electrochemical process. The electrochemical techniques of cyclic voltammetry and chronoamperometry which were employed in this work can be considered from the standpoint of electrode dimensionality.

1. <u>Cyclic Voltammetry for Diffusion Controlled Processes.</u>

Cyclic voltammetry is a useful technique for the initial characterization of electrodes. By applying a triangular voltage ramp the equivalent of three-dimensional i-t-E (current-time-potential) responses give an instantaneous qualitative picture from which to evaluate the electrode.

For the case of dimensionality equal to {2} (linear diffusion conditions), the current is proportional to the area of the electrode, concentration of the electroactive solute, and the square root of the scan rate, $v^{1/2}$ in $(V/s)^{1/2}$. The Randles-Sevcik equation for the peak current in amperes at 25°C can be used to determine the surface area of an electrode when the current function expressed as the ratio, $i_p/v^{1/2}$, is constant:

$$i_p = (2.69x10^5)n^{3/2}ACD^{1/2}v^{1/2} \qquad [6]$$

For practical reasons the scan rate range is selected for which the peak width obeys the following relationship:

$$|E_p - E_{p/2}| = 2.2\frac{RT}{nF} \qquad [7]$$

where $E_{p/2}$, the half-peak potential, is the potential at $i_p/2$.

For a spherical electrode with dimensionality of {0}, Nicholson and Shain [9] obtained an approximate relationship between the peak current and the scan rate:

$$i_p = (2.69x10^5)n^{3/2}ACD^{1/2}v^{1/2} + (0.724x10^5)\frac{nCDA}{r} \qquad [8]$$

In contrast to the linear diffusion conditions, the current function, $i_p/v^{1/2}$, for spherical diffusion is not a constant but increases as the scan rate decreases. Equation [9] can be used to calculate r and A from the slope and intercept of the linear portion of a plot of $i_p/v^{1/2}$ *vs* $v^{-1/2}$. At a sufficiently low scan rate, the voltammogram becomes sigmoidal shaped with a steady-state plateau current, i_s, which is independent of the scan rate:

$$i_s = 4\pi nFCDr \qquad [9]$$

A steady-state current only occurs for the condition of spherical diffusion and can be used to determine the radius of the spherical electrode. In the case of an ultramicrodisk electrode, when the steady-state conditions for the hemispherical diffusion are reach, the limiting current is given by

$$i_s = 4nFCDr_d \qquad [10]$$

2. Chronoamperometry for Diffusion Controlled Processes.

For electrodes with dimensionality {2}, the current-time response (chronoamperogram) to an instantaneous change of the working electrode potential for a diffusion controlled process is given by the Cottrell equation:

$$i = \frac{nFACD^{1/2}}{(\pi t)^{1/2}} \qquad [11]$$

where n is the number of electrons transferred in the electrochemical process, F is the Faraday constant in coulombs/equivalent, A is the electrochemical surface area in cm^2, and C is the bulk concentration in mole/cm^3. Equation [1] is only valid when the potential step is sufficiently negative for a cathodic process, or positive for an anodic process, such that the concentration of the electroactive species at the electrode is zero.

For electrodes with spherical geometry and electrode dimensionality of {0}, the limiting current for a diffusion controlled process is given by

$$i = \frac{nFACD^{1/2}}{(\pi t)^{1/2}} + 4\pi nFCDr \qquad [12]$$

where r is the radius of the sphere in cm. The faradaic current is the sum of a transient term proportional to the electrode area and a steady-state term proportional to the radius of the electrode. For ultramicrodisk electrodes, the steady state term becomes

$$i = 4nFCDr_d \qquad [13]$$

where r_d is the radius of the disk in cm. [10,11,12,13]. The time for the current to become constant depends on the size of the electrode, i.e., when the following condition is met:

$$\frac{1}{(\pi Dt)^{1/2}} \ll \frac{1}{r} \qquad [14]$$

The smaller the radius of the electrode, the shorter the time required to reach the steady-state condition.

b. *Electrochemically Active Surface Areas of Sensor Electrodes.*

Electrodes were evaluated in phosphate-buffered saline (PBS, 0.1 M Na_2HPO_4-NaH_2PO_4, 0.12 M NaCl, pH 7.2) electrolyte containing ~1 mM ruthenium hexaammine trichloride, $Ru(NH_3)_6Cl_3$, and in the supporting electrolyte (PBS) alone. The diffusion coefficient of the Ru hexaammine in the phosphate buffered saline electrolyte is 6.7 x 10^{-6} cm^2 sec^{-1} [14].

In the cyclic voltammetry measurements the potential of the working electrode was varied between 0.1 and -0.45 V from an initial potential of 0.0 V versus the Ag/AgCl reference electrode. The Ru complex undergoes the following reversible, one electron reaction:

$$Ru(NH_3)_6^{+3} + e^- \leftrightarrow Ru(NH_3)_6^{+2}$$

Conditions were sought and found for which sigmoidal-shaped voltammograms, characteristic of the response under spherical diffusion conditions, were observed. The range of scan rates employed was 0.002 to 10 V/sec. Within this range changes in the mass transport from spherical to semiinfinite linear diffusion were observed. Chronoamperometry measurements were made by stepping the applied potential from 0.1V to -0.45V and monitoring the current decrease as a function of time. To correct the cyclic voltammograms and chronoamperograms acquired in solutions of $Ru(NH_3)_6Cl_3$

in PBS for the charging and residual currents, background measurements over the same range of scan rates and potential ranges were measured in PBS and stored on the recorder disk. The background corrections were carried out with the Bascom-Turner microprocessor controlled recorder.

The chronoamperometric current response of large GC sensor electrodes of 3 mm and 0.6 mm diam. plotted against $t^{-1/2}$ showed "Cottrellian" behavior, i.e., such plots were linear with intercepts near zero as predicted by equation [11]. Cyclic voltammetry studies of the GC electrodes showed a constant current function over a range of sweep rates permitting the calculation of the electrochemical surface area from the Randles-Sevcik equation (equation [6]) when D and C were known.

The chronoamperometric current response of the array of microdisk electrodes plotted against $t^{-1/2}$ was linear for $t < 1$ sec and had a non-zero intercept so that the area and radius were determined from equations [12] and [13]. Cyclic voltammograms at slow sweep rates (< 20 mV sec^{-1}) were sigmoidal with the limiting current independent of sweep rate, permitting the use of equation [10] to determine the radius, r_d. In some tests, the cyclic voltammetric current function at moderate to high sweep rates (0.2 V to 5 V sec^{-1}) was constant, permitting the use of the Randles-Sevcik equation [6] to determine the area. In other tests, the current function was not constant, and equation [8] was used to determine the area and radius from the slope and intercept of the plot of $i_p/v^{1/2}$ *vs* $v^{-1/2}$. The variation in diffusion behavior of the microdisk array electrodes may be due to changes in the micro-disk surfaces and orientation as a result of polishing the sensor electrode surface prior to each test. Since the carbon fibers are randomly arranged within the epoxy filler, different surface orientations might be produced each time the surface is renewed.

The results of one series of electrochemical measurements on four microdisk array sensors are shown in Table 3. The values for the radii determined from the expression for the steady state current measured by two methods are in good agreement. However, some variation was found in the values found for the electrochemical areas. The electrochemically determined values for the radii corresponds to the sum of the radii of all elements of the array. The nominal geometric radius of the carbon fibers used in the sensors is 5 µm so that an electrochemical radius of 36 µm would correspond to a total of ~7 fibers. For the sake of comparison, the table also shows the number of fibers which were visible by optical microscopy. However, there is no guarantee that all of the visible fibers are actually exposed. The difference between the number of fibers observed and the number of fibers based on the electrochemically determined radii indicates that many of the fibers were not exposed to the electrolyte.

Table 3. Electrochemically determined dimensions of microdisk electrodes in PN_2 sensors. The electrochemical radius (r) and area (ESA) determined on the basis of: (1) the cyclic voltammetric limiting current at slow sweep rate using equation [10]; (2) the cyclic voltammetric current function, $i_p v^{-1/2}$, using Randles-Sevcik equation [6]; (3) chronoamperometric current under spherical diffusion control (equations [12], [13]).

Sensor I.D.	Probe Diameter (mm.)	No. of Visible Fibers in Probe	r (µm)	ESA (cm^2)	Method
931-97-G16	1.6	9	36.6	4.34×10^{-5}	(1)
				4.23×10^{-5}	(2)
			36.2	4.06×10^{-5}	(3)
931-99-G16	1.6	7	33.1	3.45×10^{-5}	(1)
				3.23×10^{-5}	(2)
			35.7	2.13×10^{-5}	(3)
978-7-G16B	1.6	11	39.8	4.99×10^{-5}	(1)
				5.08×10^{-5}	(2)
			37.8	3.69×10^{-5}	(3)
978-33-G20	0.9	32	78.9	1.96×10^{-4}	(1)
				1.05×10^{-4}	(2)
			71.9	1.11×10^{-4}	(3)

An array of microelectrodes has two advantages over a single microelectrode or a single large electrode. One advantage is that there is a possible ~100-fold gain in signal due to the large electrochemical surface area of the array, compared to the signal from a single microdisk electrode of 10 µ diam. and electrochemical area of ~7.85×10^{-7} cm^2. The second advantage is that the microdisk array, although having a large total electrochemical area, has the mass transport properties and low resistance polarization of microelectrodes. The latter characteristics were expected to allow shorter reaction times for the reduction reaction and Ru^{II}-N_2 complex formation, and a more rapid voltammetric waveform for quantifying uncomplexed Ru^{II}, with the combined effect being a more rapid analytical waveform for PN_2. As will be seen, these expectations were only partially fulfilled.

4.0 PERFORMANCE TESTS OF PROTOTYPE NITROGEN SENSORS

4.1 Glassy Carbon Based Sensors.

In vitro tests of membrane enclosed GC-based sensors were carried out over a range of PN_2 from 0 to 10 atm. The pseudo-first order rate constant, k′, was determined at each pressure by following the change in $[Ru^{II}]$ during a sequence of three to four 1 min reactions. Reaction sequences were repeated at 10 min intervals. The plots of ln $[Ru^{II}]$ *vs* time for one sensor are shown in Figure 6. In the presence of N_2, and following a short induction period, $[Ru^{II}]$ was observed to decrease as a result of complexation with N_2 to form Ru^{II}-N_2. At higher pressures, the slope of the ln $[Ru^{II}]$ *vs* t plots was greater due to the increased rate of disappearance of $[Ru^{II}]$. In the absence of N_2 (not shown), $[Ru^{II}]$ remained constant or increased slightly due to the reduction of additional Ru^{III}. The reproducibility of the N_2 complexation reaction is indicated by the superimposition of the ln $[Ru^{II}]$ *vs* t plots obtained at the same pressures.

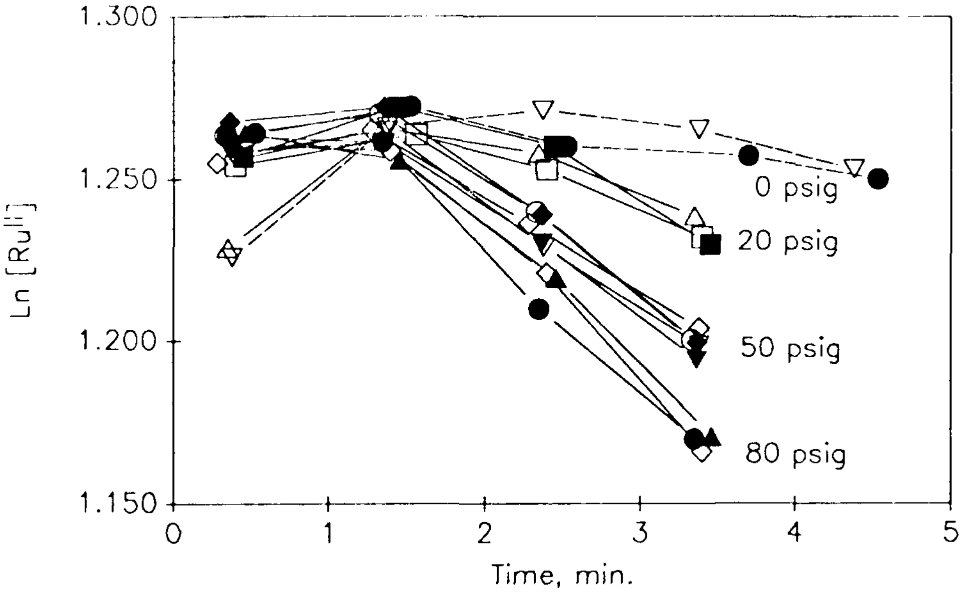

Figure 6. Plots of ln $[Ru^{II}]$ *vs* time at different PN_2.

Figure 7 shows the pseudo-first order relationship between k′ and PN_2 for the sensor reactions of Figure 6 together with analogous data obtained with other sensors. Regression correlation coefficients were 0.98-0.99. Second order rate constants derived from the slopes of these plots are given in Table 4. The M^{-1} sec^{-1} values of the rate constant are about three times higher than those reported for solution reactions indicating that separating the Ru^{II}-Nafion from the bulk environment with a gas permeable membrane does not affect the reaction kinetics adversely.

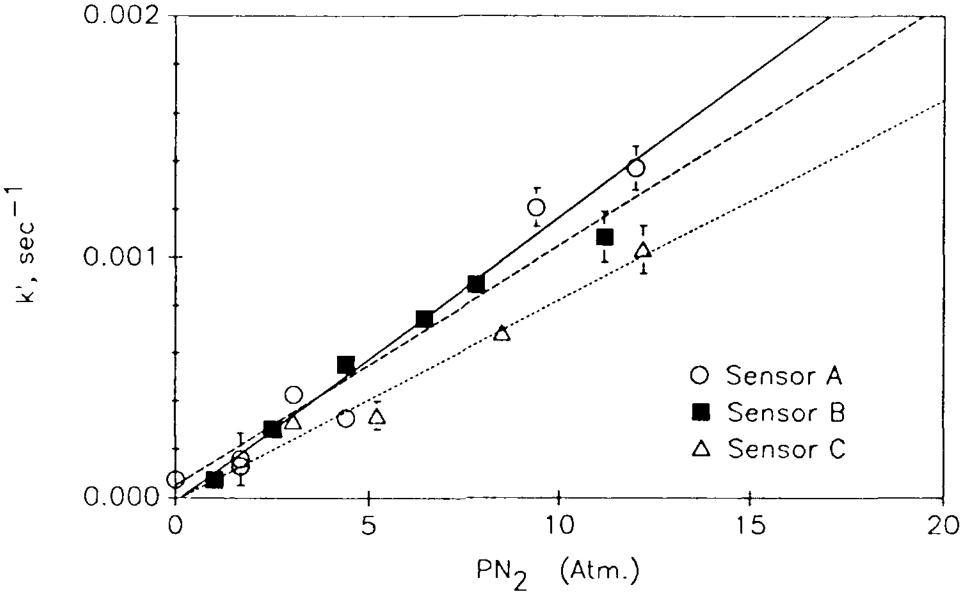

Figure 7. Plots of k′ at different PN$_2$ for sensors of different size. Slope of the lines give the second order rate constant for the formation of Ru^{II}-N$_2$. A) O---O: 3 mm diam. B) ■---■ and C) Δ...Δ: 0.6 mm diam. (each data point represents the mean of 5 measurements).

Table 4. Rate constants for Ru^{II}-N$_2$ complex formation calculated from the slopes of plots in Figure 7.

Sensor	k, atm^{-1} sec^{-1}	k, M^{-1} sec^{-1}
A	$1.18 \times 10^{-4} \pm 1.03 \times 10^{-5}$ (Average of 4 sensors)	0.19 ± 0.017
B	1.00×10^{-4}	0.16
C	8.30×10^{-5}	0.13

Figure 8 demonstrates the response of k′ to a change in the gas composition in the bulk solution. For the first 60 min of k′ measurements, the sensor was immersed in air-saturated solution. During the next 80 min 100% N$_2$ gas was passed through the solution. This was followed by a period of bubbling the solution with Ar, and finally with 100% N$_2$. The analytical protocol used three 1 min reaction periods, each followed by a voltammetric measurement of [Ru^{II}], to generate plots of ln [Ru^{II}] *vs* time from which the values of k′ were calculated. The results suggest that the bulk solution equilibrates more rapidly with N$_2$ than with Ar. However, the presence of air in the Ar gas line during the early stages of bubbling Ar through the solution cannot be discounted.

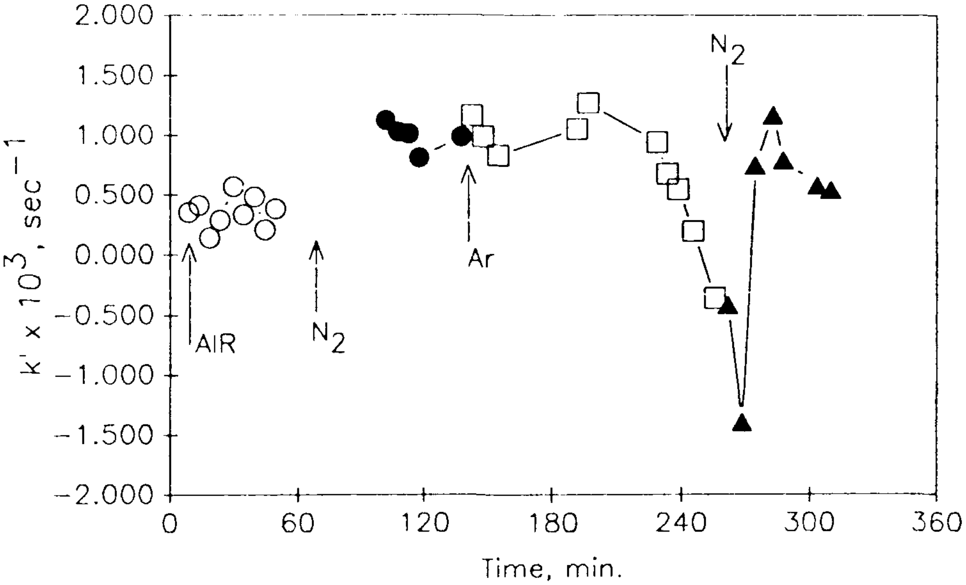

Figure 8. Response of GC-based N_2 sensor to changing gas composition. Arrows indicate time at which the input gas was changed. Each data point was determined from the slope of the line: $\ln[Ru^{II}]_t = -k't + \ln[Ru^{II}]_0$.

4.2 Carbon Fiber Based Sensors.

4.2.1 Kinetic Studies of Ru^{II}-N_2 Formation with Microdisk Array Sensors.

Continuing the experimental approach used with the large diameter sensors, kinetic studies with the microsensors were first carried out with three to four reaction periods of 1 min duration, each of which was followed by a voltammetric scan to measure the unreacted Ru^{II}. As seen in Figure 9, plots of ln $[Ru^{II}]$ *vs* time for the microsensors were very different from those obtained for the large sensors and 1 min reaction times. Whereas the large sensor demonstrated an induction period before the decrease in $[Ru^{II}]$ was observed (Figure 6), the microsensor showed an immediate and large decrease in $[Ru^{II}]$. Not only are these plots not linear, but they indicate an increase in $[Ru^{II}]$ after 3 or 4 reaction steps. The change in slope of the ln $[Ru^{II}]$ *vs* time plots suggested that the $[N_2]$ in the sensor was not constant during the entire reaction sequence, but was being depleted during the prolonged reaction time.

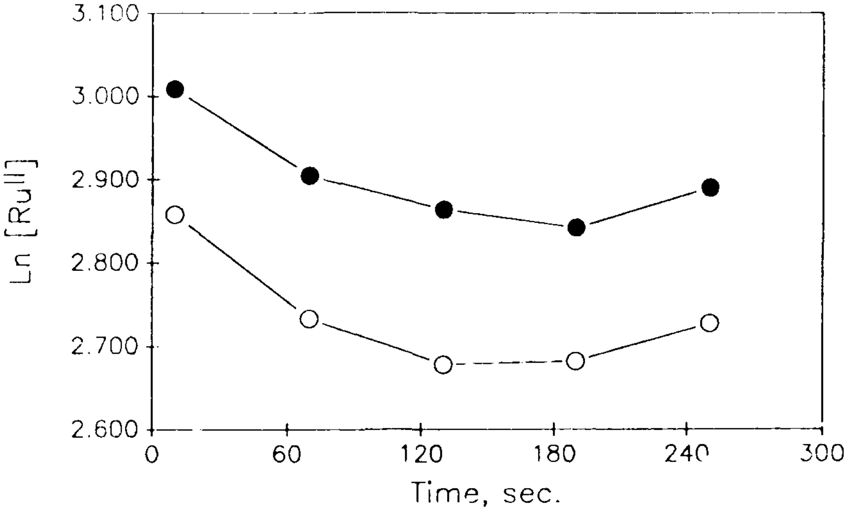

Figure 9. Plots of ln [Ru^{II}] *vs* t for test protocols having a sequence of 1 min reaction times.

Subsequent tests utilized a range of reaction times, ranging from 4 sec reactions to 20 sec reactions, to determine the minimum reaction time which would be in the time domain of pseudo-first order kinetics. When [Ru^{II}] measurements were made at 20 sec intervals, the ln [Ru^{II}] *vs* time plots were not linear, and reproducibility between successive reactions was lacking (Figure 10). The figure also illustrates the sensor response in the absence of N_2. The [Ru^{II}] increases with successive reduction steps, similar to that shown in Figure 9 when N_2 was depleted in the microenvironment surrounding the sensor.

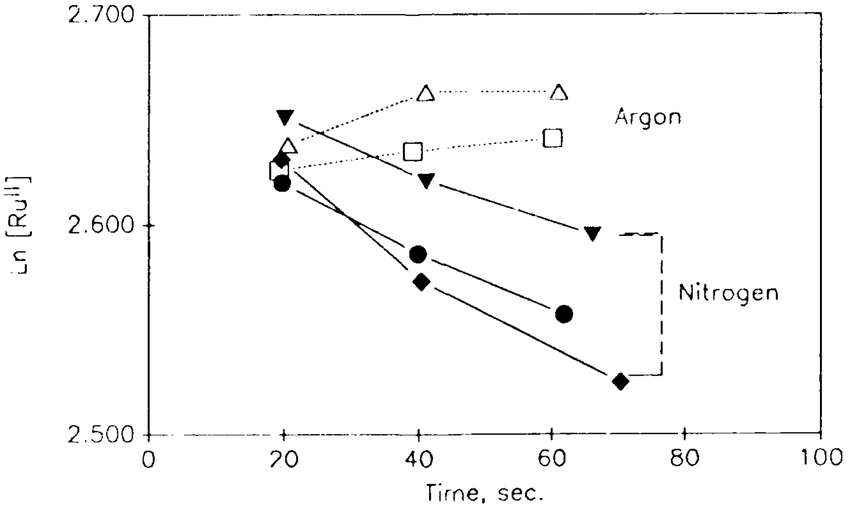

Figure 10. Plots of ln [Ru^{II}] *vs* t in the presence and absence of N_2.

When $[Ru^{II}]$ measurements were made at 4 to 6 sec intervals during a total reaction time up to ~50 sec, plots of ln $[Ru^{II}]$ vs time showed consistent pseudo-first order behavior (Figure 11). Plots shown in Figure 11 are linear from ~10 to 50 sec with regression correlation coefficients of 0.987 to 0.997.

Pseudo-first order and second order rate constants, determined from the slopes of plots shown in Figure 11B-D, are listed in Table 5. The rate constants are higher than those measured with the large sensors at the same PN_2. Several factors, physical and chemical, might contribute to this difference. Factors arising from physical differences between sensor types include the different concentrations of Nafion of the various sensors, different gas diffusion membrane and different area/volume (A/V) ratio of the electrochemical cells comprising the sensors. Another factor might be the presence in the Nafion membrane of another species in addition to N_2 which might complex with Ru^{II} and lead to an apparently higher value of k′. If some Ru^{II}-N_2 complex was produced in the sensor during preparation and preliminary test procedures, then the simultaneous formation of both mono- and binuclear nitrogen complexes of Ru^{II} during a PN_2 measurement protocol would result in artifactually high values for k′.

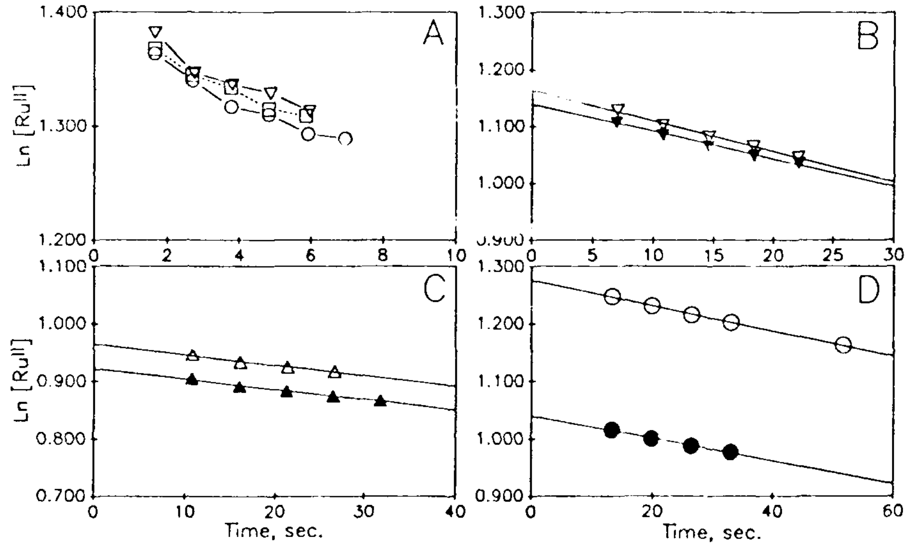

Figure 11. Plots of ln $[Ru^{II}]$ *vs* t for test protocols using short reaction times.
Regression lines are shown for B, C and D.

Table 5. Rate Constants for Formation of Ru^{II}-N_2 Complex with EIC Nitrogen Sensors.

Sensor Electrode Area (cm^2)	Nafion Volume (cm^3)	A/V (cm^{-1})	Reaction time (sec)	k′ x 10^3 (sec^{-1}) (100% N_2 at 1 atm.)	Average of all k′ values in series (x 10^3 sec^{-1})	k x 10^3 (atm^{-1} sec^{-1})	k (M^{-1} sec^{-1})[a]
[b]5 x 10^{-5}	7 x 10^{-6}	7	4.9	3.80 ± 9.02% 3.53 ± 9.78%	3.67 ± 3.7%	3.67 ± 3.7%	5.92
[b]5 x 10^{-5}	7 x 10^{-6}	7	6.6	2.89 ± 10.6% 2.63 ± 10.0% 2.51 ± 7.93% 2.05 ± 12.4%	2.52 ± 12.1%	2.52 ± 12.1%	4.06
[b]5 x 10^{-5}	5 x 10^{-6}	10	6.55	2.18 ± 3.04% 1.84 ± 6.19% 1.93 ± 5.39% 1.90 ± 3.18% 1.96 ± 6.04%	1.96 ± 6.1%	1.96 ± 6.1%	3.16
[b]5 x 10^{-5}	5 x 10^{-6}	10	5.3	1.78 ± 9.28% 1.79 ± 5.90% 2.02 ± 4.85%	1.86 ± 5.9%	1.86 ± 5.9%	3.00
[c]3 x 10^{-3}	3 x 10^{-5}	100	60	0.10 0.083	0.10 0.083	0.10 0.083	0.16 0.13
[c]7 x 10^{-2}	3 x 10^{-5}	2500	60	0.118 ± 8.3% (N=4)	0.118	0.118 ± 8.3%	0.19 ± 0.007
[d]Solution reaction	none	NA	600	.069		0.069	0.10

a. Assuming [N_2], 1 atm. = 6.2 x 10^{-4} M.
b. Sensor with microdisk carbon electrode array; diameter of each disk = 10 μm.
c. Sensor with glassy carbon electrode.
d. Reaction in solution monitored electrochemically and spectrophotometrically [5, 7].

4.2.2 Response of P_{N_2} Microdisk Array Sensors to Dynamic Conditions of Changing P_{N_2}.

The kinetic results presented in Section 4.2.1 demonstrated that the most reproducible and reliable estimate of k' is obtained from the slope of a plot of ln $[Ru^{II}]$ *vs* time providing the reaction time corresponds to the time domain of pseudo-first order kinetics. The disadvantage of this approach, in a practical sense, is the time required to perform the electrochemical measurements and analyze the data. In an effort to develop a more rapid P_{N_2} assay, the alternative approach of determining k' from the ratio of two measurements of $[Ru^{II}]$ was evaluated with the microsensors.

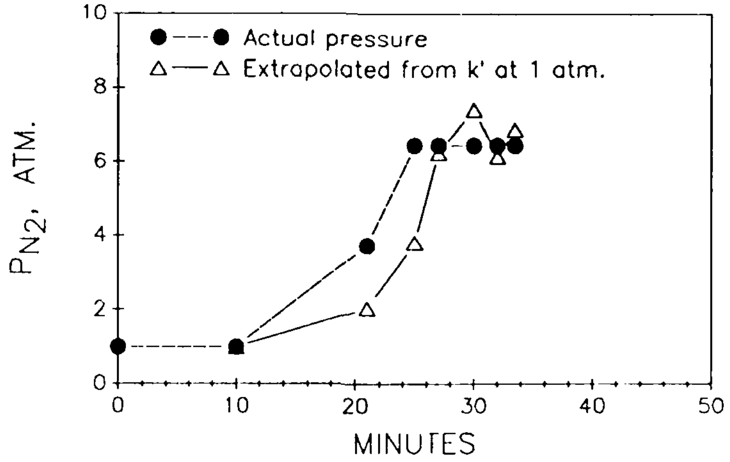

Figure 12. Response of P_{N_2} microsensor to changing N_2 pressure. Sensor was coated with 1.0 µL of 0.5% Nafion. k' was determined from $k' = \ln([Ru^{II}]_0/[Ru^{II}]_t)$. The pressure within the chamber was monitored with a Model AB Pressure Transducer (Data Instruments).

Figure 12 illustrates the change in k' with 100% N_2 and increasing pressure. In order to avoid the long time for P_{N_2} equilibration between a large volume of solution and the gas phase above it, a different test configuration was employed. For the test shown in Figure 12, the sensor was coated with 1 µL of 0.5% Nafion, and the tip of the sensor was enclosed within a three-layered covering consisting of 2 layers of porous Teflon (Goretex) with wet filter paper between them. The 3 layers were held in place with a small O-ring. The assembly was suspended in a humidified N_2 atmosphere in the pressure chamber. The k' values were determined from the ratio of two measurements of $[Ru^{II}]$ at 10 sec intervals and converted to P_{N_2} readings shown in the figure from the k' values at 1 atm or zero psig as monitored with a Data Instruments Pressure Transducer. The results demonstrate that the sensor response to rising P_{N_2} lags about 2-3 min behind the actual increase in chamber pressure. This delay may represent the time for N_2 to equilibrate across the 3-layered membrane. After equilibration at 8 atm. pressure, the sensor P_{N_2} readings fluctuated by about ± 0.5 atm. The fluctuation in equilibrium P_{N_2} readings indicates that the short method using the ratio of two Ru^{II} concentrations rather than the long method using the slope of several Ru^{II} concentrations is not the optimum protocol for measuring P_{N_2}.

4.2.3 Effect of Nafion Concentration and Film Thickness.

The kinetic studies of Ru^{II}-N_2 complex formation were carried out using sensors with Nafion membranes applied by immersing the tip of the sensor into an ethanol:water solution of 1.75% or 2.5% Nafion (wt%). In order to control the volume of the Nafion film more precisely, the coating procedure was modified so that the Nafion was applied by micropipette. The test data shown in Figure 12 were obtained with a sensor prepared with 1.0 µL of 0.5% Nafion solution applied to the cross-sectional surface of the probe to give a Nafion membrane volume of 3 nanoliters. The response of the sensor to changing PN_2 was appropriate. Other sensors prepared with less Nafion, e.g., 0.5 µL of 0.5% Nafion for a membrane volume of 1 nanoliter were less sensitive to changes in PN_2 and had a more erratic response. An example of this is given in Figure 13. Although the chamber pressure was raised to > 6 atm, the maximum PN_2 indicated by the sensor was ~4.5 atm. The physicochemical basis for the failure of sensors with ultrathin Nafion membranes to follow changes in PN_2 above ~4.5 atm. is not understood at this time. It appears that there is a minimum volume of Nafion required for a sensor to respond accurately to PN_2 changes, and the data suggest that the minimum volume is ~3 nanoliters. This is an aspect of sensor configuration which needs further study for optimal sensor performance.

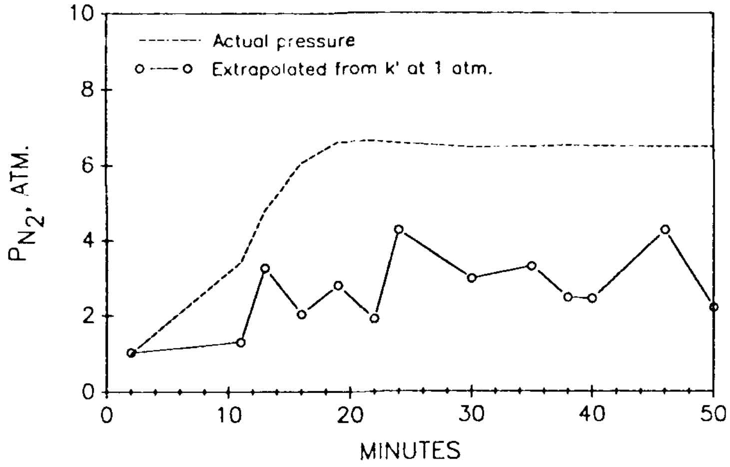

Figure 13. Response of PN_2 microsensor with a change in N_2 pressure from 1 atm to ~6 atm. Sensor was coated with 0.5 µL of 0.5% Nafion (membrane volume = ~1 nanoliter). k′ was determined from: $k' = \ln([Ru^{II}]_0/[Ru^{II}]_t)$. The pressure within the chamber was monitored with a Model AB Pressure Transducer (Data Instruments).

4.3 Comparison of Mass Transport Properties of Prototype Sensors.

The electrochemical technique of chronoamperometry was discussed in Section 3.4.2 as a method for determining the electrochemical radius and surface area of electrodes. Part of the electroanalytical waveform used for PN_2 measurement is analogous to the technique of chronoamperometry. The current-time response to the step change in potential for the reduction of Ru^{III} can be analyzed using the approach discussed in Section 3.4.1 to determine the diffusion behavior of the Ru pentaammine in the Nafion film of the sensors. Essentially the same type of graphical analysis was employed, i.e., the current response to the potential step was plotted *vs* $t^{-1/2}$, and the linearity and intercept were evaluated to identify the type of diffusion control.

For the large GC-based, Nafion-coated sensors, plots of current *vs* $t^{-1/2}$ were linear for times > 0.15 sec to 12 sec (the limit of the measurement), and had an intercept near zero, consistent with semi-infinite linear diffusion and an electrode dimensionality of {2}. In some tests, a plot of the log of the current *vs* time was linear, consistent with finite linear diffusion such as that in a thin layer cell. In contrast, the chronoamperometric response of Nafion coated microdisk array sensors resembled most closely the response expected for hemispherical diffusion at a microdisk electrode. Plots of current *vs* $t^{-1/2}$ were linear for times up to 3 sec and had non-zero intercepts. For times longer than 3 sec, a steady state current was observed, and the integral of the current-time curve, e.g., charge *vs* time, was linear.

Each modification of sensor design was undertaken with the goal of decreasing the time required to obtain a single PN_2 measurement and increasing the frequency of iterative measurements. Thus the array of microdisk electrodes was intended to enable a more rapid electrochemical waveform, and the very thin Nafion membrane was employed to decrease the volume and thickness of the electrolyte compartment to improve the equilibration time. In retrospect, it appears that the hemispherical diffusion behavior of the microdisk electrode array was detrimental to its performance as a PN_2 sensor. The steady state reduction of Ru^{III} at long potential step times, times which corresponded to the duration of the Ru^{II}-N_2 complexation reaction, meant that Ru^{II} was continually being generated during that time period, and diffusing away from the electrode rather than reaching a constant concentration. Consequently, the rate of its disappearance due solely to N_2 complex formation became increasingly difficult to quantify, and the values of k′ became more erratic. The problem might be rectified by employing a larger number of fibers and a higher concentration of Nafion in a thin film. These two changes in design will increase the effective electrode radius to provide an electrode dimensionality of {2} and improve the area/volume relationship to approach finite linear diffusion behavior.

5.0 CONCLUSIONS AND RECOMMENDATIONS FOR FURTHER DEVELOPMENT

It is clear from the previous results that the nitrogen sensor development program at EIC Laboratories has accomplished most of the requirements for a practical nitrogen sensor for studying inert gas uptake and exchange under hyperbaric conditions. A prototype sensor was fabricated with dimensions suitable for *in vivo* PN_2 measurements. A linear response to solution PN_2 from 1-10 atm was demonstrated. With an appropriate analytical waveform and data acquisition/analysis software, it should be possible to make iterative PN_2 measurements at ~40 sec intervals. A relatively small future effort would be required to modify the sensor design for improved response time, and to finalize an analytical protocol and data acquisition/data processing strategies so that the technology can be utilized by investigators engaged in hyperbaric research.

a. *Design Modifications.*

The early prototype GC-based sensors were characterized by a high A/V ratio due to a combination of the thin layer of Nafion present and the relatively large surface area of the GC electrode. Owing to the thin layer geometry, the reduction of Ru^{III} to Ru^{II} may have approximated bulk electrolysis conditions during the time of the first reduction step so that the concentration of Ru^{II} was nearly constant during the N_2-complexation reactions. In contrast to this, the reduction of Ru^{III} on the microelectrode array sensors clearly did not go to completion, but attained steady state electrolysis conditions during each reduction step. Accordingly, subsequent measurements of Ru^{II} may have reflected the loss of Ru^{II} by diffusion away from the electrode surface in addition to its reaction with N_2. The combined effects of these two processes, diffusion and complexation, may have contributed to the high values of k′ for the N_2-complexation reaction observed with the microelectrode array sensors. While the effect of each of these two processes could be sorted out with appropriate experimentation, a more practical approach would be to fabricate the microsensors so that they would have the appropriate mass transport properties as discussed in Section 4.3.

b. *Modification of Analytical Protocol.*

Reproducible values of k′ at constant PN_2 were obtained from a series of measurements of $[Ru^{II}]$ over time with k′ determined from the slope of a ln $[Ru^{II}]$ *vs* time plot. In contrast, the method of calculating k′ from the ratio of two measurements of $[Ru^{II}]$ made at short time intervals resulted in a high variability in k′. Although the two point measurement at short intervals seemed attractive for simplicity and rapidity of measurement, there is considerable sacrifice of precision and reliability. Accordingly, future development of analytical protocols will concentrate on determining k′ from regression analysis of multiple measurements of $[Ru^{II}]$. Examination of the data in Figure 10B indicates that a complete set of data points might be acquired in < 30 sec, and with appropriate software, provide a reading of k′ ~30 sec later, less than the time required to ready the sensor for another measurement cycle.

6.0 REFERENCES

1. Allen, A.D. and C.V. Senoff, J. Chem. Soc., Chem. Commun., 621, 1965.
2. Harrison, D.E. and Taube, H., J. Am. Chem. Soc. 89:5706, 1967.
3. Robblee, L.S., Development of a N_2 Sensor for *In Vivo* Measurement of PN_2 in Biological Tissues. Contract N00014-82-C-0133, 1/1/82 to 6/30/82.
4. Robblee, L.S., Development of a N_2 Sensor for Determination of PN_2 in Body Tissues. Contract N00014-83-C-0458, 6/15/83 to 6/14/86.
5. Robblee, L.S. and M.A. Parker, Final Report, Contract No. N00014-82-C-0133, "Development of Nitrogen Sensor for Determination of PN_2 in Body Tissues," July, 1982.
6. Lewis, T.J. and L.S. Robblee, In: Electrochemical Sensors for Biomedical Applications, ed. D.K.N. Li, The Electrochemical Society, Pennington, NJ, Proc. Vol. 86-14:146-159, 1986.
7. Elson, C.M., I.J. Itzkovitch and J.A. Page. Can. J. Chem. 48:1639, 1970.
8. Oldham, K.B., In: Ultramicroelectrodes, eds. M. Fleischmann, S. Pons, D.R. Rolison and P.P. Schmidt, Datatech Systems, Inc., Morganton, NC, 1987, pp. 276-288.
9. Nicholson, R.S. and I. Shain, Anal. Chem. 33:706-723, 1964.
10. Oldham, K.B., J. Electroanal. Chem. 122:1-17, 1981.
11. Aoki, K. and J. Osteryoung, J. Electroanal. Chem. 122:19-35, 1981.
12. Hepel T. and J. Osteryoung, J. Phys. Chem. 86:1406-1411, 1982.
13. Hepel T., W. Plot and J. Osteryoung, J. Phys. Chem. 87:1278, 1983.
14. Twardoch, U.M., D.V. Hills and T.L. Rose, Proc. 179th Meeting Electrochemical Society, Washington, DC, May 5-10, 1991. Extended Abstract 721.

APPENDIX

AN ELECTROCHEMICAL SENSOR FOR QUANTITATION OF TISSUE P_{N_2}

by

L. S. Robblee and M. M. Brunelle

Presented at

1991 Undersea and Hyperbaric Medical Society Annual Meeting
June 19-23, 1991
San Diego, California

AN ELECTROCHEMICAL SENSOR FOR QUANTITATION OF TISSUE PN_2.

L. S. Robblee and M. M. Brunelle
EIC Laboratories, Inc., 111 Downey Street, Norwood MA 02062.
(Undersea Biomedical Res., 18 (Suppl.):63, 1991)

In situ measurements of tissue nitrogen uptake and elimination would be of great benefit in establishing the etiology of different types of decompression sickness and in formulating decompression schedules for undersea divers. Although N_2 is not directly oxidizable or reducible in an aqueous solution, an electrochemical sensor for N_2 was developed based on the kinetics of the reaction of molecular N_2 with transition metal cations to form a stable metal-dinitrogen complex. The sensor, containing a film of the appropriate metal cation (M^{+n}) within a hydrophobic, gas-permeable membrane, is activated for measurement by applying a reducing potential to generate the N_2-complexing cation species, M^{+n-1}. After a short period of time for N_2 complex formation, a potential ramp is applied to oxidize and quantitate the uncomplexed cation. The sensor is restored to its initial state by oxidizing the N_2 complex to regenerate M^{+n} and dissociate the N_2. For the reaction, $M^{+n-1} + N_2 \rightarrow M^{+n-1}\text{-}N_2$, the pseudo-first order rate constant, $k' = k\,[N_2]$ is obtained from the slope of the plot of $\ln\,[M^{+n-1}]$ *vs* time. *In vitro* tests of sensor performance under equilibrium conditions demonstrated this linear relationship over the range of PN_2 from 1-10 atm. Under dynamic conditions of changing PN_2, the sensor response indicated that the actual concentration of N_2 in solution equilibrated slowly with changes in N_2 pressure in the gas phase above the solution. The present sensor is the size of a 15 gauge hypodermic needle and can make iterative PN_2 measurements in air saturated solution ($PN_2 = 0.77$ atm) at 3-5 min. intervals with a reproducibility of ± 5%. More frequent measurements with ± 0.5-2% reproducibility are possible at higher PN_2. Future development includes reduction in size of the sensor and modification of the analytical protocol to permit more rapid measurements at low PN_2.